Contents lists available at ScienceDirect

Communications in Nonlinear Science and Numerical Simulation

journal homepage: www.elsevier.com/locate/cnsns

Research paper

On the generalized logistic random differential equation: Theoretical analysis and numerical simulations with real-world data

V. Bevia [a],[*], J. Calatayud [b], J.-C. Cortés [a], M. Jornet [c]

[a] *Instituto Universitario de Matemática Multidisciplinar, Universitat Politècnica de València, Camino de Vera s/n, 46022, Valencia, Spain*
[b] *Department of Mathematics, Universitat Jaume I, Av. Vicent Sos Baynat, s/n, 12071, Castellón, Spain*
[c] *Department of Mathematics, Universitat de València, Dr Moliner 50, 46100, Burjassot, Spain*

ARTICLE INFO

ABSTRACT

Based on the previous literature about the random logistic and Gompertz models, the aim of this paper is to extend the investigations to the generalized logistic differential equation in the random setting. First, this is done by rigorously constructing its solution in two different ways, namely, the sample-path approach and the mean-square calculus. Secondly, the probability density function at each time instant is derived in two ways: by applying the random variable transformation technique and by solving the associated Liouville's partial differential equation. It is also proved that both the stochastic solution and its density function converge, under specific conditions, to the corresponding solution and density function of the logistic and Gompertz models, respectively. The investigation finishes showing some examples, where a number of computational techniques are combined to construct reliable approximations of the probability density of the stochastic solution. In particular, we show, step-by-step, how our findings can be applied to a real-world problem.

1. Introduction

This paper is a contribution to the field of random differential equations. These are defined as classical differential equations whose coefficients and initial conditions are random variables or stochastic processes, and the solution is a differentiable stochastic process [1–3]. Due to the existence of different types of limits in probability theory, such solution may have different interpretations: sample-path, mean-square, etc. The sample-path notion, which refers to the trajectories of the solution, is the weakest and the usual one in a computational setting [1,4–7]

The statistical content of the solution is of interest. When the interest relies on the moments, different techniques may be used: Monte Carlo simulation, based on sampling and calculating the statistics of the sample; perturbation expansions, based on Taylor's expansions around a parameter with a certain radius of convergence; generalized polynomial chaos expansions, constructed from orthogonal polynomials; etc. [8,9]. On the other hand, for the explicit computation of the probability density function (PDF), the Random Variable Transformation (RVT) technique has been of use in the literature when a closed-form solution exists [10–12]. This method has been applied to the solution of the logistic random differential equation [13,14]. A complementary approach is based on the resolution of the Liouville's partial differential

---

* Corresponding author.
  E-mail addresses: vibees@upv.es (V. Bevia), calatayj@uji.es (J. Calatayud), jccortes@imm.upv.es (J.-C. Cortés), marc.jornet@uv.es (M. Jornet).

equation (PDE) [15–19]. A recent application of Liouville's equation can be found for the Gompertz random differential equation [20].

The logistic differential equation has been generalized in different senses to better modeling the dynamics of real-world phenomena where it has been applied. This generalization has included its reformulation in terms of fractional derivatives; the substitution of the contagion rate term by a power-law function, etc. [21–23]. In this paper, we deal with the following generalization of the logistic differential equation

$$Y'(t) = AY(t)\left(1 - \left(\frac{Y(t)}{K}\right)^B\right), \quad t \geq t_0, \quad Y(t_0) = Y_0. \tag{1.1}$$

As usual, t is interpreted as the time. The parameter A is the growth rate, K is the carrying capacity, and B is a power that controls how fast the limiting number K is approached. When $B = 1$, the classical logistic differential equation is obtained. And when B tends to 0, the Gompertz equation is given. Indeed, given $A, B > 0$, we put $\hat{A} = AB$, and then (1.1) can be written as

$$Y'(t) = \frac{\hat{A}}{B}Y(t)\left(1 - \left(\frac{Y(t)}{K}\right)^B\right). \tag{1.2}$$

Now, let us calculate the limit as $B \to 0^+$ of the following term that defines the right-hand side of the above equation:

$$\lim_{B \to 0^+} \frac{\left(1 - \left(\frac{Y(t)}{K}\right)^B\right)}{B} = \lim_{B \to 0^+} -\left(\frac{Y(t)}{K}\right)^B \ln\left(\frac{Y(t)}{K}\right) = -\ln\left(\frac{Y(t)}{K}\right) = \ln\left(\frac{K}{Y(t)}\right).$$

As a consequence, as $B \to 0^+$, the differential equation (1.1) can be expressed as

$$Y'(t) = \hat{A}Y(t)\ln\left(\frac{K}{Y(t)}\right),$$

which corresponds to the Gompertz model [24,25]. The incorporation of the power B allows for more flexible S-shaped curves to model growth phenomena over time. Examples of application include tumor growth [26–29] and diseases such as SARS [30,31], dengue fever [32], influenza H1N1 [33], Zika [34], Ebola [35], and COVID-19 [36–39].

We investigate the random counterpart of (1.1), in order to extend the previous literature on the logistic random differential equation [13,14] and the Gompertz random differential equation [20]. It is assumed that $B > 0$, $K > 0$, $Y_0 \in [0, K]$ (almost surely) and A are random variables on a common underlying and complete probability space $(\Omega, \mathcal{F}, \mathbb{P})$. Due to uncertainty propagation, the solution $Y(t)$ is a differentiable stochastic process. The randomness of the parameters arises from the uncertainty inherent to the problem that in principle cannot be reduced by additional knowledge [9].

The organization of the remaining part of the paper is the following. In Section 2, the sample-path and mean-square solution to (1.1) is rigorously found. In Section 3, the PDF of the solution is obtained in two ways, by the RVT technique and by solving the Liouville's PDE. In Section 4, the behavior of the solution, when the power tends to 1 or 0, is examined (through the mean-square convergence and also via the convergence of the densities) to replicate the deterministic counterpart. In Section 5, we illustrate our main findings with two examples that include a real-world application. Finally, in Section 6, the main conclusions are drawn.

2. Stochastic solution

In this section, we investigate the existence and uniqueness of a stochastic solution to the generalized logistic random differential equation model (1.1). Two notions of solution are treated: sample-path solution and mean-square solution.

2.1. Sample-path solution

It is known that $Y(t)$ is a sample-path solution to (1.1) if Y is a stochastic process [i.e. measurable from $(\Omega, \mathcal{F})$ to $(\mathbb{R}, \text{Borel sets})$ for each $t \geq t_0$] and its trajectories solve (1.1) on $[t_0, \infty)$ in a deterministic sense [2, chapter 3], [1, Appendix I]. The construction of the sample-path solution is usually straightforward; one merely solves the deterministic problem and checks that the conditions for being a sample-path solution (measurability and common time domain for the trajectories) are satisfied.

In the present case, model (1.1) corresponds to a Bernoulli differential equation. After the standard change of variables $X = Y^{-B}$, a linear differential equation is derived for X. At the end, the solution to (1.1) becomes

$$Y(t) = \frac{K}{\left[1 + \left(-1 + \left(\frac{K}{Y_0}\right)^B\right)e^{-AB(t-t_0)}\right]^{1/B}}. \tag{2.1}$$

When $0 \leq Y_0 \leq K$ almost surely $Y(t)$, which is defined by (2.1), is the sample-path solution and it lies within $[0, K]$ almost surely, for every $t \geq t_0$.

2.2. Mean-square solution

It is known that $Y(t)$ is a mean-square solution to (1.1) when the derivative in (1.1) (and in general any limit) is considered in the metric of the Lebesgue space $L^2(\Omega, d\mathbb{P})$, [2, chapter 4], [1,3]. This space is Hilbert with the inner product $(Y_1, Y_2) \mapsto \mathbb{E}[Y_1 Y_2] = \int_\Omega Y_1 Y_2 \, d\mathbb{P}$, where $\mathbb{E}$ denotes the expectation operator. It consists of the random variables with finite variance. The norm of $L^2(\Omega, d\mathbb{P})$ is denoted by $\| \cdot \|_2$. Mean-square convergence is of great interest because convergence in this setting implies convergence of the two most sought moments of a stochastic process: the mean and the variance [1].

Among the remaining Lebesgue spaces ($L^p(\Omega, d\mathbb{P})$, $\| \cdot \|_p$), the case $p = \infty$, whose norm $\| \cdot \|_\infty$ corresponds to the almost surely least upper bound (essential supremum), will be needed.

Let us see that the sample-path solution defined by (2.1) is also the mean-square solution on $[t_0, \infty)$, whenever $\| A \|_\infty < \infty$, $B > 0$ almost surely, $\| B \|_\infty < \infty$, $0 \le Y_0 \le K$ almost surely, and $0 < \kappa_0 \le K \le \kappa_1 < \infty$ almost surely, where κ_0 and κ_1 are constant.

Let

$$F(Y, \omega) = A(\omega)Y \left(1 - \left(\frac{Y}{K(\omega)}\right)^{B(\omega)}\right), \quad Y \in [0, K(\omega)], \quad \omega \in \Omega.$$

Fix an $\omega \in \Omega$. By the triangular inequality and the mean value theorem, it is easy to see that $F(\cdot, \omega)$ is Lipschitz on $[0, K(\omega)]$, with Lipschitz constant $\| A \|_\infty (1 + \kappa_1 \| B \|_\infty /\kappa_0)$:

$$
\begin{aligned}
|F(Y_1, \omega) - F(Y_2, \omega)| &= \left| A(\omega)Y_1 \left(1 - \left(\frac{Y_1}{K(\omega)}\right)^{B(\omega)}\right) - A(\omega)Y_2 \left(1 - \left(\frac{Y_2}{K(\omega)}\right)^{B(\omega)}\right) \right| \\
&\le |A(\omega)| \| Y_1 - Y_2| \left(1 - \frac{Y_1}{K(\omega)}\right)^{B(\omega)} \\
&\quad + |A(\omega)||Y_2| \left| \left(1 - \frac{Y_1}{K(\omega)}\right)^{B(\omega)} - \left(1 - \frac{Y_2}{K(\omega)}\right)^{B(\omega)} \right| \\
&\le \| A \|_\infty |Y_1 - Y_2| + \| A \|_\infty |Y_2| \frac{\| B \|_\infty}{\kappa_0} |Y_1 - Y_2| \\
&\le \| A \|_\infty \left(1 + \frac{\kappa_1 \| B \|_\infty}{\kappa_0}\right) |Y_1 - Y_2|.
\end{aligned}
$$

By Tietze extension theorem [40, Th. 1], $F(\cdot, \omega)$ can be extended to a Lipschitz map $\tilde{F}(\cdot, \omega) : \mathbb{R} \to \mathbb{R}$ with Lipschitz constant $\| A \|_\infty (1 + \kappa_1 \| B \|_\infty /\kappa_0)$. Consider $Y'(t) = \tilde{F}(Y(t))$. By [2, Th. 4.3], [1, Th. 5.1.2], the Lipschitz condition on the whole $\mathbb{R}$ implies that the problem $Y'(t) = \tilde{F}(Y(t))$, $Y(t_0) = Y_0$, possesses a unique mean-square solution on $[t_0, \infty)$. Any mean-square solution is equivalent to the sample-path solution [41, Th. 3(a)], which is (2.1) precisely. Then (2.1) is the mean-square solution. This completes the proof.

3. Two methods for computing the PDF of the solution stochastic process

In this section, we compute the PDF of $Y(t)$, denoted as $f_{Y(t)}(y)$. By definition, the PDF is a non-negative Borel measurable function characterized by $\mathbb{P}[Y(t) \in \mathcal{B}] = \int_\mathcal{B} f_{Y(t)}(y) \, dy$ for any Borel set $\mathcal{B}$ in $\mathbb{R}$. Two complementary techniques are employed: the application of the RVT method and the resolution of the Liouville's PDE. The former requires the computation of a Jacobian, while the latter needs the resolution of the continuity equation. The computation of the PDF is advantageous since it allows for the computation of any one-dimensional moment

$$\mathbb{E}[(Y(t))^k] = \int_{-\infty}^{\infty} y^k f_{Y(t)}(y) \, dy, \quad k = 1, 2, \ldots, \tag{3.1}$$

provided it exists. In particular, the mean (case $k = 1$) and the variance (from $k = 2$), $\mathbb{V}[Y(t)] = \mathbb{E}[(Y(t))^2] - (\mathbb{E}[Y(t)])^2$.

3.1. First method: RVT technique

Let (Y_0, K, A, B) be an absolutely continuous random vector with a certain joint probability distribution, $f_{(Y_0, K, A, B)}$. Fix $t \ge t_0$. To apply the technique, we need a transformation that relates the inputs, (Y_0, K, A, B), to the output, $Y(t)$. The transformation mapping is the following:

$$g(Y_0, K, A, B) = \left(\frac{K}{\left[1 + \left(-1 + \left(\frac{K}{Y_0}\right)^B\right) e^{-AB(t-t_0)}\right]^{1/B}}, K, A, B \right),$$

where the auxiliary components K, A and B have been conveniently chosen. The inverse mapping is computed easily:

$$h(Y, K, A, B) = \left(\frac{K}{\left[1 + \left(-1 + \left(\frac{K}{Y} \right)^B \right) e^{AB(t-t_0)} \right]^{1/B}}, K, A, B \right).$$

The Jacobian of h is the determinant of the matrix of first partial derivatives of h:

$$Jh(Y, K, A, B) = \frac{\partial Y_0}{\partial Y} = \frac{K^{1+B} e^{AB(t-t_0)}}{Y^{B+1} \left[1 + \left(-1 + \left(\frac{K}{Y} \right)^B \right) e^{AB(t-t_0)} \right]^{1/B+1}} > 0.$$

Such positivity holds because $0 < Y < K$ and $B > 0$ almost surely. By the RVT formula [12], [42, Th. 2.1.5], and after marginalizing with respect to K, A and B, the PDF of $Y(t)$ is obtained in a semi-implicit manner through a triple integral:

$$f_{Y(t)}(y) = \int_{\mathcal{D}_{(K,A,B)}} f_{(Y_0, K, A, B)} \left(\frac{K}{\left[1 + \left(-1 + \left(\frac{K}{Y} \right)^B \right) e^{AB(t-t_0)} \right]^{1/B}}, K, A, B \right)$$
$$\times \frac{K^{1+B} e^{AB(t-t_0)}}{Y^{B+1} \left[1 + \left(-1 + \left(\frac{K}{Y} \right)^B \right) e^{AB(t-t_0)} \right]^{1/B+1}} \, dK \, dA \, dB. \tag{3.2}$$

Here $\mathcal{D}_{(K,A,B)}$ denotes the support of (K, A, B).

The PDF (3.2) is the general formula. Sometimes, it may be simplified. First, if Y_0, K, A and B are independent random variables, then the joint PDF $f_{(Y_0, K, A, B)}$ factorizes:

$$f_{(Y_0, K, A, B)} = f_{Y_0} \times f_K \times f_A \times f_B.$$

In consequence, the PDF of the solution can be expressed via an expectation

$$f_{Y(t)}(y) = \int_{\mathcal{D}_B} \int_{\mathcal{D}_A} \int_{\mathcal{D}_K} f_{Y_0} \left(\frac{K}{\left[1 + \left(-1 + \left(\frac{K}{y} \right)^B \right) e^{AB(t-t_0)} \right]^{1/B}} \right) f_K(K) f_A(A) f_B(B)$$
$$\times \frac{K^{1+B} e^{AB(t-t_0)}}{y^{B+1} \left[1 + \left(-1 + \left(\frac{K}{y} \right)^B \right) e^{AB(t-t_0)} \right]^{1/B+1}} \, dK \, dA \, dB$$
$$= \mathbb{E} \left[f_{Y_0} \left(\frac{K}{\left[1 + \left(-1 + \left(\frac{K}{y} \right)^B \right) e^{AB(t-t_0)} \right]^{1/B}} \right) \frac{K^{1+B} e^{AB(t-t_0)}}{y^{B+1} \left[1 + \left(-1 + \left(\frac{K}{y} \right)^B \right) e^{AB(t-t_0)} \right]^{1/B+1}} \right].$$

Note that this is a parametric approximation of the PDF because it is obtained as an expectation of a transformation of the input random variables (A, B, K). This PDF representation is beneficial since Monte Carlo simulation can be easily applied by sampling the involved random variables and then computing the expectation that approximates the PDF [43].

Secondly, if an input random variable (Y_0, K, A or B) is discrete, rather than absolutely continuous, its PDF may be viewed in a generalized sense. For example, if K is discrete, then

$$f_K(k) = \sum_i k_i \delta_0(k - k_i),$$

where $k_i > 0$ are the mass points of the discrete random variable K and δ_0 is the Dirac delta function (everywhere zero but with infinite value at the origin and integral equal to 1). The integral over $\mathcal{D}_K$ would become a sum over the points $\{k_i\}_i$.

3.2. Second method: Liouville's PDE

The procedure and the notation from [20] are replicated. Let us denote model (1.1) as

$$Y'(t) = g(Y(t), K, A, B),$$

where

$$g(Y, K, A, B) = AY \left(1 - \left(\frac{Y}{K} \right)^B \right). \tag{3.3}$$

This g, and later h, are different to those from the previous subsection, and match with [20]. The Liouville's PDE for the joint PDF of $(Y(t), K, A, B)$, $f_{(Y(t),K,A,B)}(y, K, A, B)$, is

$$\frac{\partial f(y, K, A, B)}{\partial t} + \frac{\partial \{f(y, K, A, B)g(y, K, A, B)\}}{\partial y} = 0,$$

where the notation $f := f_{(Y(t),K,A,B)}$ was used in order to shorten the expression. Such partial derivative with respect to y is the divergence operator in dimension one. By computing the derivative of the product in the second summand, we can obtain an alternative and useful formulation of the Liouville's PDE,

$$\frac{\partial f(y, K, A, B)}{\partial t} + g(y, K, A, B) \frac{\partial f(y, K, A, B)}{\partial y} = -f(y, K, A, B) \frac{\partial g(y, K, A, B)}{\partial y}. \tag{3.4}$$

The explicit solution to the Liouville's equation is [1, Chapter 6]

$$f_{(Y(t),K,A,B)}(y, K, A, B) = f_{(Y_0,K,A,B)}(Y_0, K, A, B) \exp \left(- \int_{t_0}^t \frac{\partial g}{\partial Y}(Y(\tau), K, A, B) \, d\tau \right) \Bigg|_{Y_0 = h^{-1}(y,K,A,B,t)},$$

where $Y(t) = h(Y_0, K, A, B, t)$ is the input–output relation and

$$Y_0 = h^{-1}(Y, K, A, B, t) = \frac{K}{\left[1 + \left(-1 + \left(\frac{K}{Y} \right)^B \right) e^{AB(t-t_0)} \right]^{1/B}}$$

is the inverse relation, in terms of the initial condition. The partial derivative of g with respect to Y is

$$\frac{\partial g}{\partial Y} = A \left(1 - \left(\frac{Y}{K} \right)^B \right) - \frac{AB}{K^B} Y^B.$$

An important term in the solution of the Liouville's PDE is

$$\exp \left(- \int_{t_0}^t \frac{\partial g}{\partial Y}(Y(\tau), K, A, B) \, d\tau \right) = e^{-A(t-t_0)} \frac{\left(K^B + (-1 + e^{AB(t-t_0)}) Y_0^B \right)^{(1+B)/B}}{K^{1+B}}.$$

Then the Jacobian of the RVT formula is retrieved as

$$\exp \left(- \int_{t_0}^t \frac{\partial g}{\partial Y}(Y(\tau), K, A, B) \, d\tau \right) \Bigg|_{Y_0 = h^{-1}(y,K,A,B,t)} = \frac{K^{1+B} e^{AB(t-t_0)}}{Y^{B+1} \left[1 + \left(-1 + \left(\frac{K}{Y} \right)^B \right) e^{AB(t-t_0)} \right]^{1/B+1}}.$$

Thus, after marginalizing the calculated $f_{(Y(t),K,A,B)}(y, K, A, B)$ with respect to K, A and B, it is obtained the PDF (3.2) as well.

4. Convergence when the power tends to 1 or 0

By the deterministic theory, it is known that the classical logistic and Gompertz differential equations are retrieved when $B = 1$ and $B \to 0$, respectively. The aim of the present section is to extend those results to the random scenario. Different convergence measures for $Y(t)$ are used: mean-square convergence and convergence of densities.

4.1. Mean-square convergence

We investigate the mean-square convergence of $Y(t)$. Two cases are distinguished, according to the probabilistic convergence of B:

- Case $B \to 1$ or $B \to 0$ almost surely. By the deterministic theory, it is known that $Y(t)$ converges to the logistic curve or the Gompertz curve almost surely when $B \to 1$ or $B \to 0$ almost surely, respectively. It is also known that $0 \le Y(t) \le K \in L^1(\Omega, d\mathbb{P})$, and analogously for the logistic and the Gompertz curves. By the dominated convergence theorem [44, result 11.32, p. 321], the almost sure convergence of $Y(t)$ translates into mean-square convergence. In conclusion, $Y(t)$ converges to the logistic curve or the Gompertz curve in the mean-square sense when $B \to 1$ or $B \to 0$ almost surely.

- Case $B \to 1$ or $B \to 0$ in the mean-square sense. Pick any sequence $\{B_n\} \to 1$ or $\{B_n\} \to 0$ in the mean-square sense. There exists a subsequence such that $\{B_{n_l}\} \to 1$ or $\{B_{n_l}\} \to 0$ almost surely. By the previous item, the corresponding $\{Y_{n_l}(t)\}$ converges in mean-square to the logistic curve or to the Gompertz curve, respectively. At the end, this implies that $Y(t)$ converges to the logistic curve or the Gompertz curve in the mean-square sense when $B \to 1$ or $B \to 0$ in mean-square.

4.2. Convergence of densities

We prove that, if $B \to 1$ or $B \to 0$ almost surely, then $f_{Y(t)}(y)$ converges to the PDF of the logistic curve or the PDF of the Gompertz curve almost everywhere, respectively. Almost everywhere convergence of densities is a strong mode of convergence, as it implies convergence in $L^1(\mathbb{R}, \mathrm{d}y)$ by Scheffé's lemma [45, p. 55], [46].

For the proof, it is assumed that Y_0 and (K, A, B) are independent, $A > 0$ almost surely (increasing trend), $Y_0 \geq z > 0$ almost surely (z constant), $\parallel B \parallel_\infty < \infty$, there exists $C > 0$ such that $f_{Y_0}(y) \leq \min\{C/y, C/y^{1+\|B\|_\infty}\}$ for all $y > 0$, and $\mathbb{E}[e^{A\|B\|_\infty(t-t_0)}] < \infty$ (finite moment-generating function of A). Due to the independence, the PDF (3.2) is rewritten as

$$
f_{Y(t)}(y) = \mathbb{E}\left[f_{Y_0}(R_B)(R_B)^{1+B} e^{AB(t-t_0)} \frac{1}{y^{B+1}} \right],
$$

where

$$
R_B = \frac{K}{\left[1 + \left(-1 + \left(\frac{K}{Y} \right)^B \right) e^{AB(t-t_0)} \right]^{1/B}}
$$

and the domain is $y \geq z$. Now,

$$
0 \leq f_{Y_0}(R_B)(R_B)^{1+B} e^{AB(t-t_0)} \frac{1}{y^{B+1}} \leq C e^{A\|B\|_\infty(t-t_0)} \min\left\{ \frac{1}{z}, \frac{1}{z^{1+\|B\|_\infty}} \right\},
$$

where such upper bound is a constant that, in consequence, belongs to $L^1(\Omega, \mathrm{d}\mathbb{P})$. The dominated convergence theorem [44, result 11.32, p. 321] allows for interchanging the limit on B and the expectation.

5. Numerical examples and real data

In this section, the previous theoretical findings will be applied to analyze the dynamics of the solution stochastic process to the random generalized logistic model (1.1), through its PDF and main moments (mean and variance). This analysis is first performed via two numerical examples, and afterward using real-world data. As several numerical challenges may appear when solving model (1.1), we shall also recall a number of deterministic and probabilistic tools that will be used in the examples.

Section 5.1 deals with the description of a numerical scheme based on the Lagrangian form of the Liouville's PDE. It is formulated in the case of deterministic coefficients and extended to the case of random coefficients. Afterward, in Sections 5.2–5.4, a brief presentation of a fast computational technique based on adaptive mesh generation and wavelets (wavelet compression-based adaptive mesh refinement); a metaheuristic optimization algorithm (Particle Swarm Optimization algorithm) and a method to construct reliable PDFs from sampled information (Principle of Maximum Entropy) will be given, respectively. Finally, in Sections 5.5 and 5.6, an application of the numerical procedures to some numerical examples and a full study of a real-world case of microbial growth data will be discussed, respectively.

5.1. Lagrangian form of the Liouville's PDE

It is well known that first order PDEs whose dynamical behavior is dominated by convection, such as the Liouville's equation, may be analyzed by the evolution of the equation solution in certain curves, called characteristic curves [47, Sec. 3.2]. The formulation of the problem in such a way is called the Lagrangian formulation of the PDE [48]. We point out that throughout this section the previous notation, $f_{Y(t)}(y)$, for the PDF of the solution for the generalized logistic model (1.1) will be conveniently adapted to our new setting in order to stress the dependence of the new quantities that will appear. This will be underlined in due course.

The Lagrangian formulation is different than the classical, fixed-mesh and Eulerian formulation of a PDE. When computing a numerical solution of a PDE, both the time domain and the space domain must be discretized, and the discretized values of the PDE at each point in the discretized space domain (mesh, or grid) are updated in each timestep. Lagrangian methods, however, treat the discretized values of the initial PDE state as individual particles that move as defined by the *velocity, or field*, function, defined by $g(y; K, A, B)$ in (3.3) in our case, and change their inherent quantity accordingly (in this case, the PDF f).

In the case of the Liouville's PDE, we can transform its classical, or Eulerian formulation (3.4), to its Lagrangian formulation in the following way:

$$
\frac{\mathrm{d}}{\mathrm{d}s} y(s; K, A, B) = g(y(s; y_0); K, A, B), \quad y(t_0) = y_0, \tag{5.1}
$$

$$
\frac{\mathrm{d}}{\mathrm{d}s} f(y(s; y_0), s \mid K, A, B) = -f(y(s; y_0), s \mid K, A, B) \frac{\partial g}{\partial y}(y(s; y_0); K, A, B). \tag{5.2}
$$

Therefore, the family of curves $\{y(s; y_0)\}_{y_0 \in \mathbb{R}}$ are the *characteristic curves*, written in the so-called *Lagrangian coordinates* $(s; y_0)$. As it can be seen, they are determined by the flow function, $g(y; K, A, B)$, in the form of an ODE given by (5.1). The

second Eq. (5.2), which defines the change of the PDF through each characteristic curve, can be solved in an exact way using the method of separation of variables

$$f_{Y(t)}(y) = f(y(t; y_0), t \mid K, A, B) = f_0(y_0) \exp\left\{ -\int_{t_0}^{t} \frac{\partial g}{\partial y}(y(\tau; y_0); K, A, B)\, d\tau \right\}. \tag{5.3}$$

As emphasized with the former notation, this expression is another representation of the PDF of $Y(t)$, which is equivalent to (3.2). As expression (5.3) shows, the time evolution of the PDF only depends on the computation of the integral through each of the characteristic curves. However it is not always possible to compute the integral in an exact way. And even if it is possible, the resulting function may be too unstable for a computer to efficiently handle. This is what often happens when carrying out computations for the generalized logistic model as it shall be illustrated in the examples.

When dealing with random coefficients, another step must be done. Particularly, an interpolation into a common grid of all conditional PDFs, $f(y, t \mid K, A, B)$, must be computed regularly after some time steps in the simulation. Afterward, all that is left is to compute the marginal PDF with respect to these random parameters in the common grid points

$$f_{Y(t)}(y) = \int_{\mathbb{R}^3} f(y, t \mid K, A, B) f_{K,A,B}(K, A, B)\, dK\, dA\, dB.$$

For the numerical computation of the solution to the system formed by (5.1)–(5.2), or equivalently, the Eqs. (5.1) and (5.3), any ODE integrator can be used. We have used the Runge–Kutta 4 (RK4) scheme, and the Simpson rule for the computation of the integral in (5.3) [49]. The time step used for the simulations shown in this section has been determined heuristically, by comparing one simulation with a certain time step and another one with half its time step. We then choose a time step after which there is no noticeable improvement. In Sections 5.5 and 5.6, we specify the particular time step used in this contribution.

5.2. Wavelet compression-based AMR

Dynamical systems such as the generalized logistic equation model (1.1) have many interesting properties, such as asymptotic stability. This means that the system converges to a specific state or value. Suppose the asymptotic state is deterministic or a random variable with a small variance. Then, the PDF will evolve into a function with very narrow support, or in 1-dimensional models such as the one studied in the present contribution, it may converge to a Dirac delta distribution. Asymptotic stability may pose a problem when computing its PDF via its related Liouville's PDE through numerical schemes.

Despite using a Lagrangian method for the PDF computation, an underlying grid in which the particles' positions and values are initialized at each time step is required, as explained in the previous subsection. In order to have a reliable computation of the evolution of the PDF, even at times values when the random system approaches its steady-state, a very high resolution, i.e., very fine grid must be chosen. However, a high-resolution grid would only be truly useful near the steady state PDF, whereas an unnecessarily high computational cost is forced in all previous time steps. This may lead to an unaffordable computational burden.

These kinds of problems, also known as multi-scale problems [50], appear in a wide variety of fields, especially in computational fluid dynamics. This problem has been addressed by using Adaptive Mesh Refinement (AMR) techniques. There are many AMR procedures; however, we have used the so-called wavelet-based AMR technique. We refer to [50] for further details on how it is practically used.

5.3. PSO algorithm

The Particle Swarm Optimization (PSO) algorithm is an optimization algorithm widely used in cases where the parameters to be optimized are not in a discrete set. In short, it generates a number of particles (combinations of possible optimal values) where a certain fitness function (FF) is evaluated. Taking into account the values of the FFs at those points, the particles are updated by imitating the behavior of birds when searching for food [51]. We will take advantage of this optimization technique to search for the best estimates for model parameters in the subsequent examples.

5.4. Principle of Maximum Entropy (PME)

There are various ways of assigning distributions to random variables or vectors. One of them is the so-called Principle of Maximum Entropy (PME [52] or MaxEnt [53]). This data-driven method seeks to obtain a PDF that captures the maximum uncertainty (which is measured by the so-called *Shannon Entropy functional*) from the available sampled information (usually described via the moments such as the mean, variance, etc.) about the random variable [54]. In this contribution we will only use the mean and variance, since adding more moments does not change the resulting PDF noticeably in this case. In Section 5.6, this method is applied to assign a PDF to a set of real data.

Mathematically speaking, we want to compute the following:

$$f_{\text{sample}} = \arg\max\left\{ \int_{\mathcal{D}} f(y)\log(f(y))\, dy \mid f \in L^1(\mathcal{D}),\ f \geq 0 \right\},$$
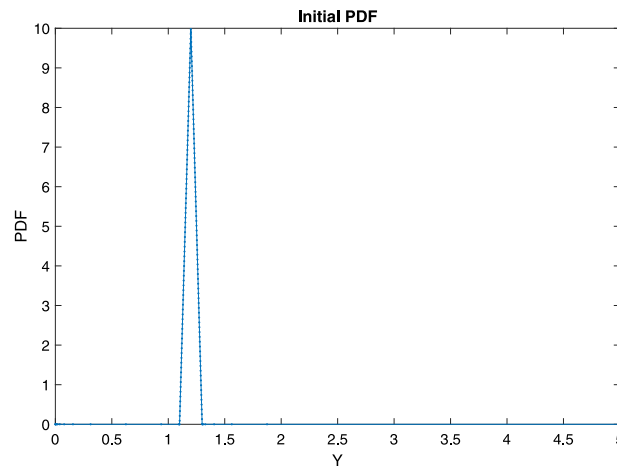
Fig. 1. Triangular distribution PDF used as initial condition for both numerical examples in Section 5.5.

Table 1
Parameter values used in Case 1 (A_1, B_1, K_1) and Case 2 (A_2, B_2, K_2), respectively. Numerical example.

	Case 1			Case 2		
Parameter	A_1	B_1	K_1	A_2	B_2	K_2
Value	0.33	1	5	0.33	2.5	5

subject to the following constraints

$$\begin{aligned} \int_{\mathcal{D}} f(y)\mathrm{d}y &= 1, \\ \int_{\mathcal{D}} y f(y)\mathrm{d}y &= \mu_{\text{sample}}, \\ \int_{\mathcal{D}} y^2 f(y)\mathrm{d}y &= \sigma^2_{\text{sample}} + \mu^2_{\text{sample}}. \end{aligned}$$

Here $\mathcal{D}$ denotes the domain of the random variable Y. Using the Lagrange multiplier method, it can be shown that the PDF has the following form [55]

$$f_{\text{sample}}(y) = \exp\{-1 - \lambda_0 - \lambda_1 y - \lambda_2 y^2\},$$

where λ_0, λ_1 and λ_2 are the *Lagrange multipliers*. These values are determined by solving the system defined by the constraints, which usually requires numerical methods since it is often nonlinear in λ_0, λ_1 and λ_2.

5.5. Numerical example

In this section, we will take advantage of the mathematical tools summarized in Sections 5.1–5.4 to compute and visualize the dynamical behavior of the PDF of the solution stochastic process for the generalized logistic model (1.1). We will assume that $t_0 = 0$ and that t is measured in hours. First, two numerical examples will be shown in order to introduce a brief idea about how the numerical solution performs. Then we will solve an inverse problem with real-world data. All computations in the following sections have been performed in an AMD Ryzen 5800H-based laptop computer with 16 GB of RAM.

5.5.1. Deterministic coefficients

Only the initial condition is assumed a random variable which follows a symmetric triangular distribution with parameters 1.1, 1.3, whose mode is located at 1.2. It can be seen in Fig. 1. The rest of model parameters, A, B and K, are assumed deterministic. We have considered two scenarios, Case 1 and Case 2, where only the value of B differs (see Table 1). In this way, we can better observe the role that parameter B plays in the model (this can repeated for the rest of model parameters). It is important to note, however, that the support of the PDF must be contained inside the interval $[0, K]$ in all times; that is, $\text{supp}\{f([0, +\infty), \cdot)\} \subset [0, K]$. This is due to the nature of the model, which assumes that K is the carrying capacity, or asymptotic equilibrium state. We have chosen our initial high resolution grid to consist of 4096 points. Figs. 2 and 3 show the time evolution of the PDF in Cases 1 and 2, respectively, along with the mean and standard deviation functions, computed from the PDF by means of (3.1). The whole computation took about 0.6 s.

Note that there are some similarities between both simulations. In particular, we can see that both simulations converge to a stationary value (the carrying capacity, $K = 5$) and their standard deviations decay to zero as this happens. This is to be expected because of the fact that the mean-square solution of the random IVP is also a pathwise solution
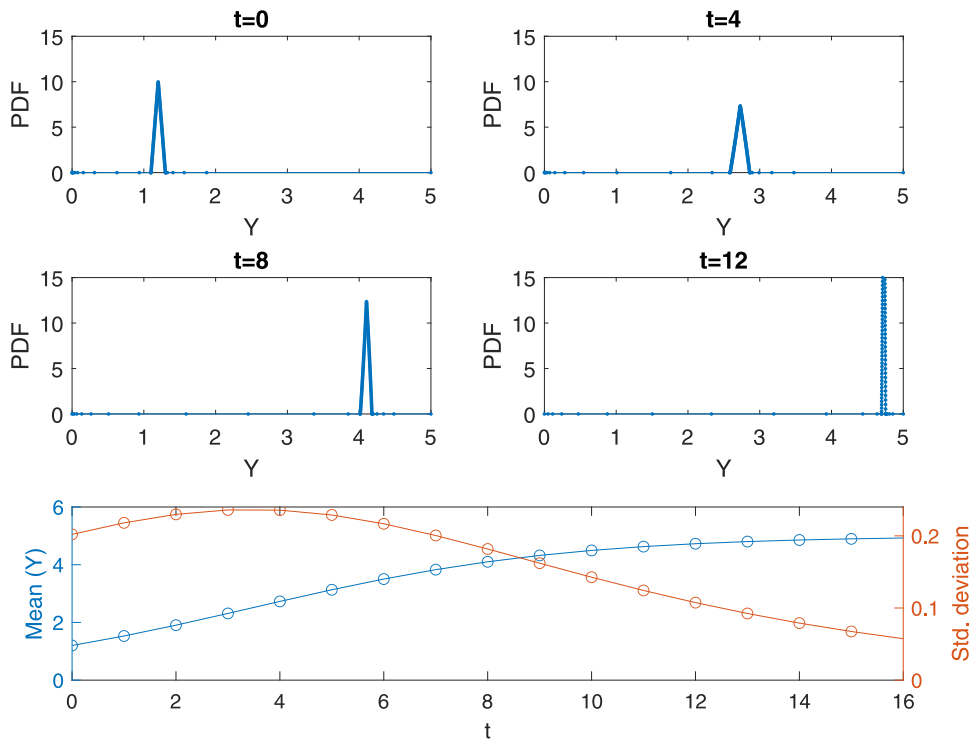
Fig. 2. Top four panels: PDF of the solution stochastic process to the generalized logistic equation model (1.1) at different time instants (in hours). Bottom panel: Mean (blue, left axis) and standard deviation (orange, right axis) of the solution stochastic process. Case 1 (Numerical Example). Maximum absolute error in the PDF total mass: $\sim 5.3 \cdot 10^{-4}$.
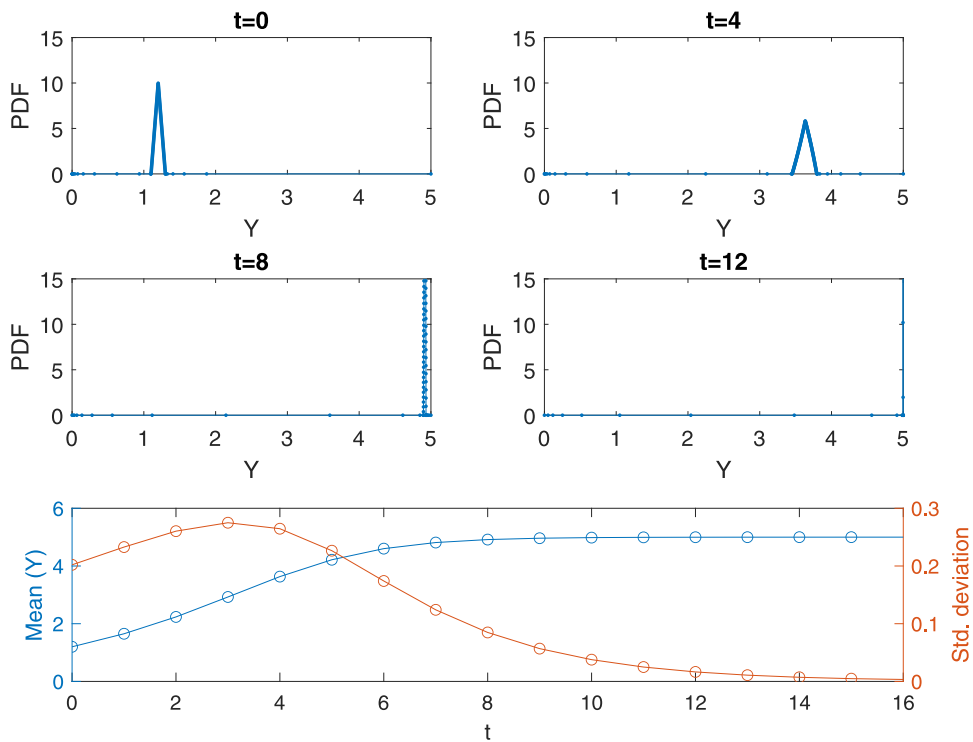

Fig. 3. Top four panels: PDF of the solution stochastic process to the generalized logistic equation model (1.1) at different time instants (in hours). Bottom panel: Mean (blue, left axis) and standard deviation (orange, right axis) of the solution stochastic process. Case 2 (Numerical Example). Maximum absolute error in the PDF total mass: $\sim 6.1 \cdot 10^{-3}$.

Table 2

Time at which measurements are taken with the mean of the measurements. 28 measurements were taken at each time. The variance was only computed in the first time, in order to use the PME. Measurements were obtained by specialized fluorescent imaging techniques whose measurement units are known as Optical Density (OD). More details about the data and how it was collected in [56]. Real-world example.

Time (h)	Mean (OD)	Time (h.)	Mean (OD)
0.000	0.286	3.547	0.527
0.233	0.308	3.828	0.547
0.465	0.331	4.061	0.558
0.698	0.354	4.294	0.569
1.001	0.383	4.527	0.581
1.234	0.403	4.759	0.590
1.466	0.416	4.992	0.597
1.839	0.437	5.275	0.608
2.072	0.450	5.508	0.612
2.304	0.464	5.740	0.616
2.537	0.476	6.039	0.616
2.849	0.486	6.271	0.617
3.081	0.500	6.503	0.617
3.315	0.514	6.803	0.619

Table 3

Lagrange's multipliers obtained in the PME method (see Section 5.4 for further details about the computation of the Lagrange's multipliers). Real-world Example.

λ_0	λ_1	λ_2
443.84321	-3132.90787	5470.16958

of the random IVP. The carrying capacity is a globally asymptotically stable state of both the logistic and the generalized logistic equations. This means that, independently of the initial value and the values for $A > 0$ and $B > 0$, all paths corresponding to the realizations of both the initial condition and the coefficients will approximate the carrying capacity value as time goes on. It is also noteworthy that the integral of the PDF, in the whole domain, is very close 1 at every timestep. This property of the PDF has been used to check the numerical approximations of the PDF when solving the Liouville's PDE are reliable at every timestep.

There also are some differences between both scenarios. In Case 1, it can be seen how standard deviation has a smooth growth and posterior decay to zero. Also, the mean curve shows a very gentle logistic-type curve, as it was expected due to the theoretical development in previous sections. However, Case 2, where the deceleration parameter is increased to 2.5, shows a sharper growth and decay of the standard deviation. Correspondingly, the mean curve stabilizes much faster than in Case 1.

5.6. Real-world example

In this subsection, we are going to apply the theoretical and numerical concepts and findings discussed in previous sections to a real data set regarding the growth of a biological culture studied at [56]. Measurements were obtained by specialized fluorescent imaging techniques whose measurement units are known as Optical Density (OD). The means of the measurements at each measured time can be seen in Table 2. All details about the biological and experimental procedures can be found at [56].

By applying the PME technique to the data regarding the set of measurements at time $t_0 = 0$, we assign an initial PDF with the form described in Section 5.4. Particularly, we remind that the PDF has the form

$$f_0(y) = \exp\{-1 - \lambda_0 - \lambda_1 y - \lambda_2 y^2\}, \tag{5.4}$$

where the λ_i are the ones defined in Table 3. In Fig. 4, we have plotted this PDF. It has been calculated by the wavelet compression-based adapted mesh. It can clearly be seen where there is a higher concentration of points. These points are obtained exactly where the function has a larger gradient.

5.6.1. Deterministic coefficients

First, the deterministic parameter values are determined in order to have a first, expected representation of the sample data. Since the PDE computation time is relatively fast, we can use the PSO algorithm directly from the PDE itself. The computational procedure used for this purpose consists of the following steps, and it is shown in the flowchart depicted in Fig. 5:
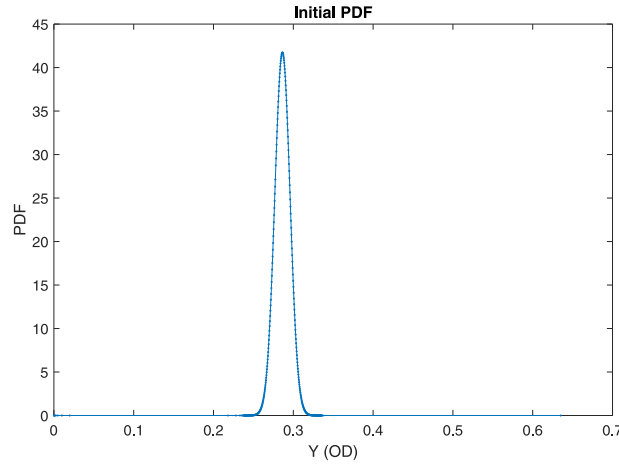
Fig. 4. PDF at $t_0 = 0$ used as the initial condition for the Liouville's PDE (see expression (5.4) and Table 3). Initial high resolution grid of 4096 points. Adapted grid with 330 points. Real-world Example.

1. Extract growth data from the data set, $\mathbf{Y}_i$, at each time measurement t_i. At this point we have a collection of 24 measurements per time instant, with a total of 28 measurements; that is, we have $\{(t_i, \mathbf{Y}_i)\}_{i=1}^{28}$, where $\mathbf{Y}_i = (Y_i^1, \ldots, Y_i^{24})$.

2. Compute the initial density, f_0, in its adapted grid $\mathcal{G}_0$ (see Section 5.2), using the PME (see Section 5.4). Also, compute the mean of the measurement vectors, $\overline{Y}_i = \frac{1}{24} \sum_{j=1}^{24} Y_i^j$ at each time instant t_i, $i = 1, \ldots, 28$. At this point, we have the initial PDF, $f_0(\mathcal{G}_0)$, and the curve of the sample means $\{(t_i, \overline{Y}_i)\}_{i=1}^{28}$.

3. We now enter the PSO algorithm (see Section 5.3). In the present work, we have used 60 particles and a maximum of 100 iterations. The parameter values used for the evaluation of the error function may be computed in two different ways depending on whether it is the first iteration or not.

   - In the first case, 60 points are generated at random positions in the parameter space; that is, $\{(A_l, B_l, K_l)\}_{l=1}^{60}$.
   - In the latter case, the same number of points are generated following a very specific set of rules [51], returning the updated set of parameter values $\{(A_l', B_l', K_l')\}_{l=1}^{60}$.

4. After the set of parameter values has been defined (let it be at the first iteration or after an update), we compute the numerical solution of the PDF at each of the time instants $\{t_i\}_{i=1}^{28}$ using the Lagrangian approach (see Section 5.1). At this point we have a family of PDFs and their corresponding adapted grids; that is, $\{f(\mathcal{G}_i, t_i \mid A, B, K)\}_{i=1}^{28}$ for each tuple of parameter values $(A, B, K) \in \{(A_l, B_l, K_l)\}_{l=1}^{60}$. Note that we have dropped the conditional PDF notation in the following steps for the sake of simplicity.

5. For each of the PDFs defined as in the previous step, we compute their respective expectations, given by Eq. (3.1) and denoted by $\{\overline{f(\mathcal{G}_i, t_i)}\}_{i=1}^{28}$, and compute its absolute error respect to the sample mean $\overline{Y}_i$ at each time instant t_i. We then compute the sum of these absolute errors; that is

$$\text{Error} = \sum_{i=1}^{28} |\overline{f(\mathcal{G}_i, t_i)} - \overline{Y}_i|.$$

6. Now, if the following absolute error

$$\text{Error} = \sum_{i=1}^{28} |\overline{f(\mathcal{G}_i, t_i)} - \overline{Y}_i|$$

varies below a given threshold, among all generated (A, B, K), which the authors have chosen as 10^{-9}, we keep the tuple of parameter values with the best fitness function value, (A^*, B^*, K^*). If not, we update the set of parameter values and we start at point (3) of the present description.

The optimal values obtained as the PSO procedure output, as defined in Fig. 5, can be found in Table 4. Fig. 6 shows the numerically computed PDF using the optimal values collected in Table 4. 60 particles were used in order to compute an optimum and the PSO ended after 100 iterations with an error tolerance of 10^{-9}. It is worth noting that the whole optimization procedure takes about 9 minutes to compute in an AMD Ryzen 7 5800H, whereas the simulation itself takes around 0.4 s to carry out calculations (no parallel computations were performed). Both cases were simulated with a $\Delta t = 0.005$ time step in the Lagrangian method. We refer to Fig. 6 for more information.
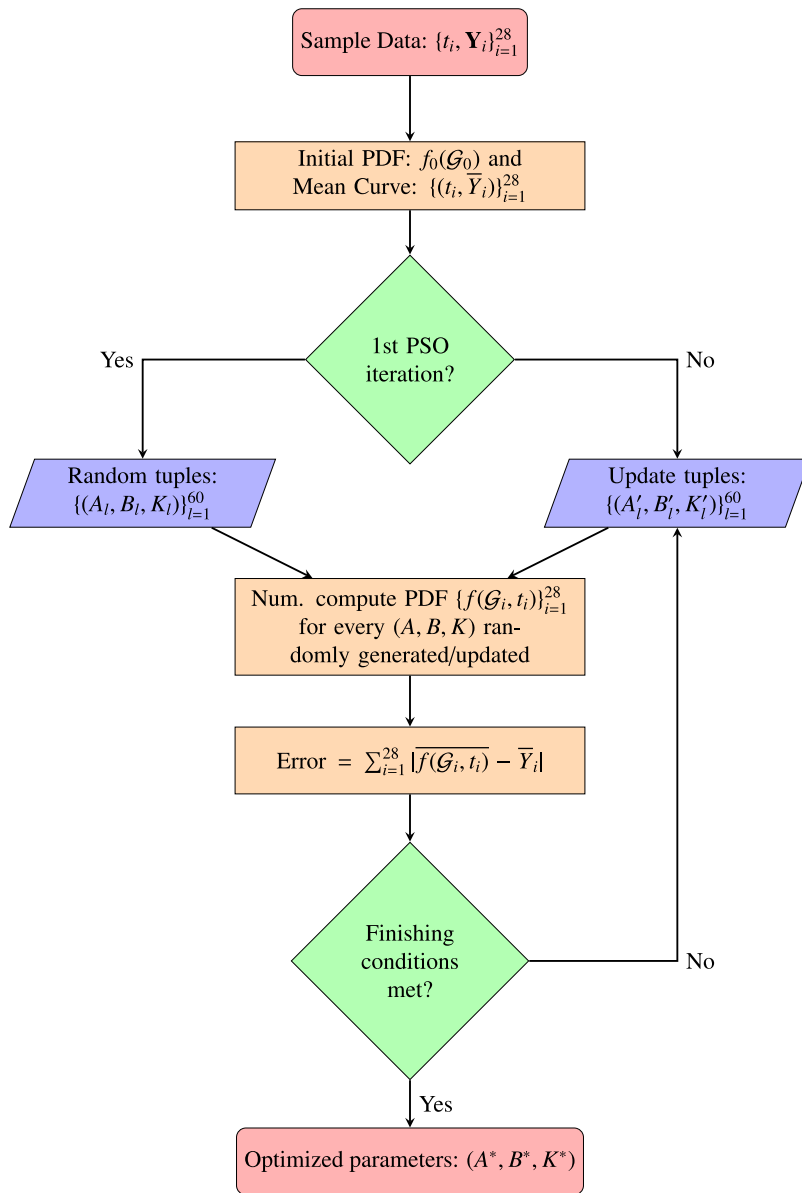
Fig. 5. Flowchart describing the entire PSO-based optimization procedure for deterministic parameters. Real-world Example with deterministic parameters.

Table 4
Optimal model parameters. Real-world example with deterministic parameters.

A^*	B^*	K^*
0.4911	1.5212	0.635

Note that the objective function to be minimized by the PSO is not necessarily convex, so no global minimum is assured. Therefore, the parameter tuple given by the PSO algorithm may not be the global minimum of the error function defined in step 6 of the procedure explanation. However, as seen in Figs. 6–8, they provide a parameter vector that allows approaching the real data with reasonable accuracy. In Fig. 7 we have plotted the average or sample mean of the sample data together with the mean and a confidence interval constructed as mean plus/minus 3 standard deviations both obtained from repeatedly solving the Liouville's PDE sampling the initial condition from its PDF, $f_0(y)$. We can observe
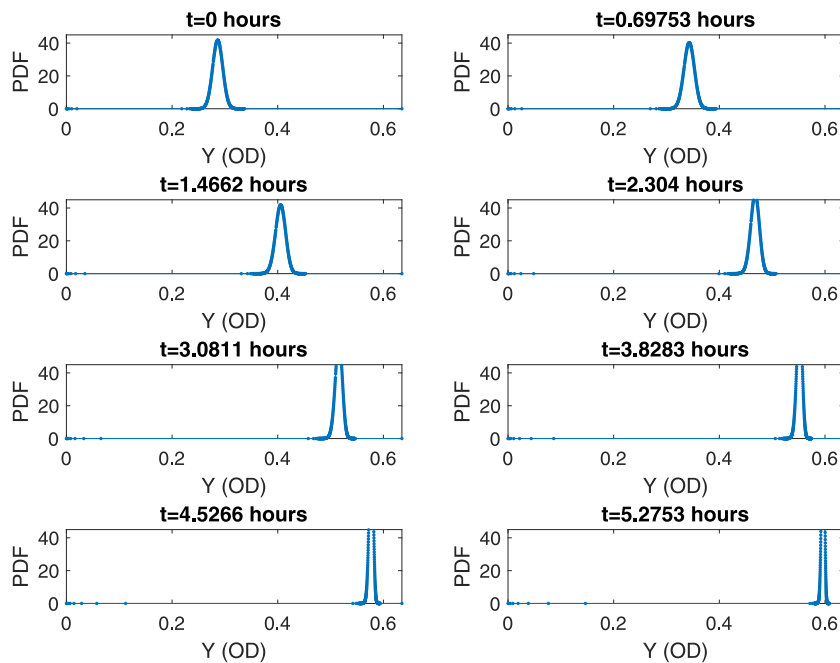
Fig. 6. Time evolution of the PDF with model parameters given in Table 4. Real-world Example with deterministic parameters. Maximum absolute error in the PDF total mass: $\sim 6.7 \cdot 10^{-4}$.
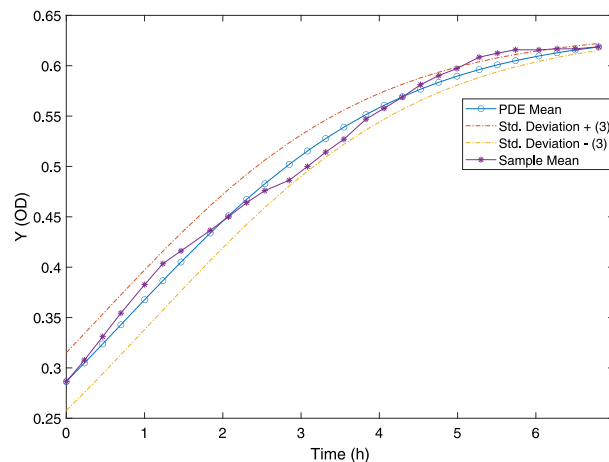

Fig. 7. Mean of the PDF obtained by solving the Liouville's PDE along with a confidence interval centered at the mean with a 3 standard deviation radius. Starry points denote the sample mean at each of the time instants. Real-world Example with deterministic parameters.

that this confidence interval captures most of the uncertainty at every time instant and, when computing the integral in the corresponding intervals, we obtain values of approximately 0.9, so we are representing a confidence interval of 90%.

Finally, in Fig. 8, absolute and relative errors between the mean computed from sampled data and the Liouville's PDF are shown. Notice that graphical representations shown in Figs. 7 and 8 are in full agreement. It is interesting to see the oscillation of the error functions in Fig. 8 which shows that, for this particular data set, we have an appropriate fit given by the generalized logistic model. We have obtained a parameter vector that allows us to represent the expected behavior of the biological population under study. Non-oscillatory error functions would be given by a fit that is always above (over-predicting), or below (under-predicting), the mean curve. This would mean that the generalized logistic model is incapable of representing the dynamics of this data set appropriately. Moreover, as the biological culture approaches its steady state, we will have a lower variability and, in theory, the amplitude will eventually decrease and stabilize.
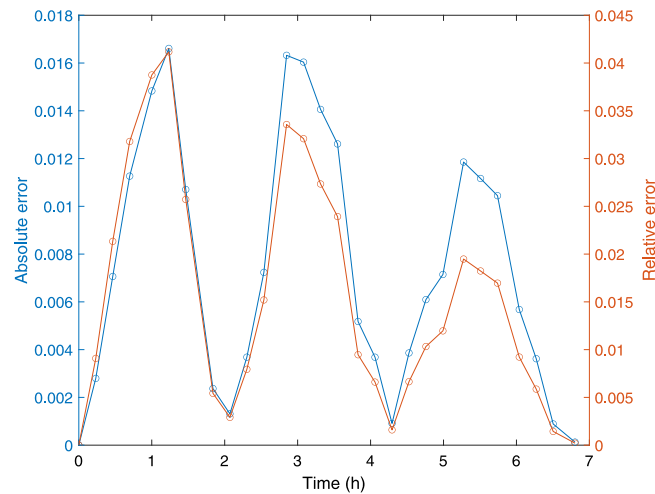
Fig. 8. Absolute error (left axis, blue curve) and relative error (right axis, orange curve) of the mean of the PDF computed by the Liouville's PDE with respect to the sample data. Real-world Example with deterministic parameters.

5.6.2. Random coefficients

In order to perform realistic simulations taking into account the uncertainty in model parameters, probability distributions are assigned in such a way that the expectation of these distributions match their corresponding deterministic optimal values collected in Table 4. In our subsequent calculations, this will be assumed for model parameters A and B, that is,

$$A^* = \int_\Omega A(\omega) \, d\mathbb{P}(\omega), \quad B^* = \int_\Omega B(\omega) \, d\mathbb{P}(\omega),$$

while $K = K^* = 0.635$ will be taken as the deterministic optimal value (see Table 4) since from its own biological interpretation its variability is negligible with respect to the one of A and B.

Probability distributions for A and B have been assigned following particular biological reasons. They are assigned a priori in such a way that the support of their corresponding PDFs makes sense in this biological problem; for example $A > 0$ and $B > 0$. Particularly, we have chosen $A \sim \mathrm{Exp}(1/A^*)$ and $B \sim \mathrm{Unif}(B^*(1 - 0.15), B^*(1 + 0.15))$; that is, an Exponential distribution whose expectation is A^* (recall that the mean of an exponential distribution is the inverse of its parameter) and a Uniform distribution centered at B^* with a 15% support radius interval, respectively.

Now, simulations of the full 28 time values of Table 2, that is, up to time 6.803 h, are computed. Fig. 9 shows the simulated PDFs at several time instants. Full simulation with random coefficients and a 4096-point base grid was performed in just over 37 min, with a timestep of $\Delta t = 0.005$.

As previously indicated, note that we have assumed the carrying capacity to be a constant, $K = K^* = 0.635$. Also note in Figs. 10 and 11 that the optimization procedure returned a set of parameters that allows a very good description of the sample data with the distributions chosen for A and B. As in the case of the deterministic coefficients, we can observe an oscillation of the error functions which again is a sign of a coherent fit to the mean data curve. Notice that there is a slight difference in the amplitude of the oscillations. This difference is natural and it is because of the nature of both problems. The case of deterministic coefficients consists in obtaining the PDF of a stochastic process depending on a single random variable, that is, the initial condition. The second case, which is represented in Figs. 10 and 11, consists in obtaining the PDF of a stochastic process where 3 of its parameters are random variables. Moreover, the relationship between the solution stochastic process and its parameters is nonlinear. This is reflected in the evolution of its PDF as it can be seen when comparing Figs. 7 and 8 with 10 and 11.

6. Conclusion

With the aim of extending recent studies performed for the logistic random differential equation and the Gompertz random differential equation, in this paper we have investigated the generalized logistic random differential equation. This equation includes a power term into the classical logistic model, to better control how fast the limiting capacity is approached. We have assumed that the parameters are random variables. Then, we have obtained the sample-path and mean-square solution rigorously, and we have computed its Probability Density Function by applying the Random Variable Transformation technique and the Liouville's equation. We have analyzed how the model reduces to the classical logistic equation and the Gompertz equation when the power tends to 1 and 0 in a probabilistic sense.
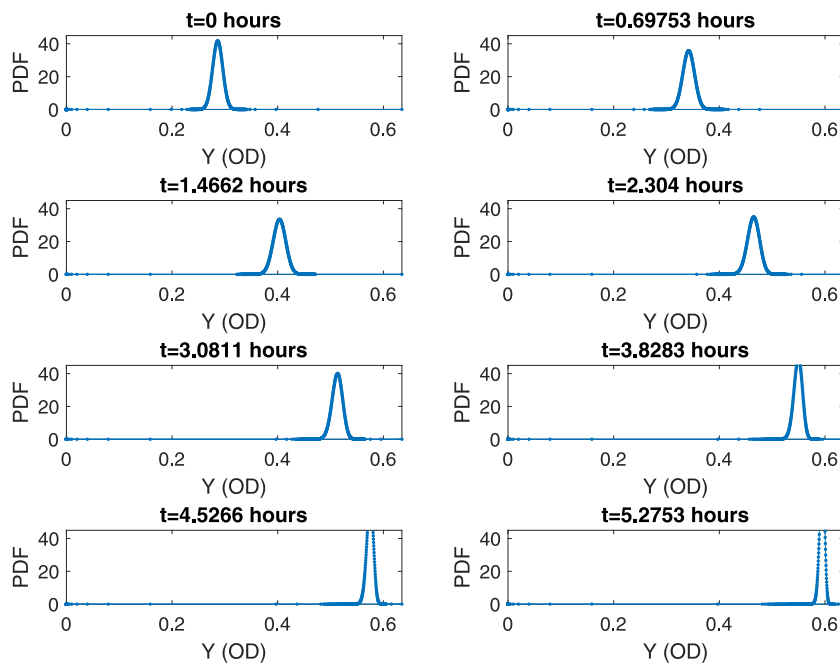
Fig. 9. Time evolution of the PDF. Real-world Example with random parameters. Maximum absolute error in PDF mass: $\sim 4.8 \cdot 10^{-5}$.
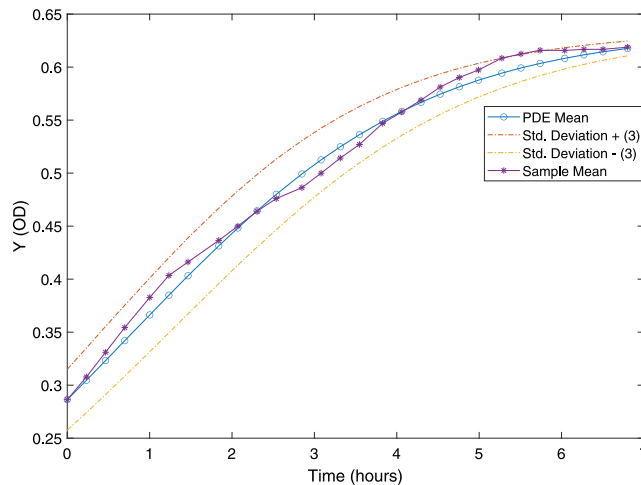

Fig. 10. Mean of the PDF obtained by solving the Liouville's PDE along with a confidence interval centered at the mean with a 3 standard deviation radius. Starry points denote the sample mean at each time instant. Real-world Example with random parameters.

Furthermore, we have made use of a type of numerical methods specially suited for the computation of the solution of partial differential equations such as Liouville's equation, where convection is the main dynamical behavior of the solution. It has first been applied to a case with deterministic coefficients and it has been extended to the scenario where coefficients are given by random variables. Afterward, an optimization procedure based on the Particle Swarm Optimization algorithm has been implemented. Its objective has been to obtain the deterministic coefficient values which allow describing the mean behavior of the biological culture growth data set.

Further research includes the full theoretical and numerical study of other growth models with uncertain parameters. Likewise, the improvement in the computational methodology used in this contribution is a main objective of the authors. Specifically, accelerating the computation of solutions to the Liouville equation using graphics cards, and extending these methods to a multidimensional setting are some of the main goals. This will further allow us to explore the potential and limitations of the methodology exposed in this contribution.
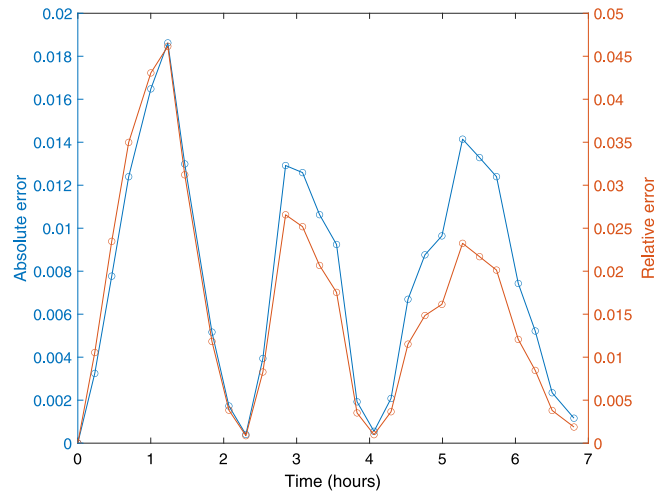
Fig. 11. Absolute error (left axis, blue curve) and relative error (right axis, orange curve) of the mean of the PDF computed by the Liouville's PDE with respect to the sample data. Real-world Example with random parameters.

CRediT authorship contribution statement

V. Bevia: Conceptualization, Software, Formal analysis, Investigation, Writing – original draft, Writing – review & editing, Visualization. **J. Calatayud:** Conceptualization, Formal analysis, Investigation, Writing – original draft, Writing – review & editing. **J.-C. Cortés:** Conceptualization, Investigation, Writing – review & editing, Supervision, Funding acquisition, Project administration. **M. Jornet:** Conceptualization, Formal analysis, Investigation, Writing – original draft, Writing – review & editing.

Declaration of competing interest

The authors declare that they have no known competing financial interests or personal relationships that could have appeared to influence the work reported in this paper.

Funding

References

[1] Soong TT. Random differential equations in science and engineering. New York: Academic Press; 1973.
[2] Neckel T, Rupp F. Random differential equations in scientific computing. Walter de Gruyter; 2013.
[3] Villafuerte L, Braumann CA, Cortés JC, Jódar L. Random differential operational calculus: theory and applications. Comput Math Appl 2010;59(1):115–25.
[4] Caraballo T, Colucci R, López-de-la-Cruz J, Rapaport A. A way to model stochastic perturbations in population dynamics models with bounded realizations. Commun Nonlinear Sci Numer Simul 2019;77:239–57. http://dx.doi.org/10.1016/j.cnsns.2019.04.019.
[5] Caraballo T, López-de-la-Cruz J, Rapaport A. Modeling random fluctuations in biological systems: application to the chemostat model with two species. IFAC-PapersOnLine 2019;52(26):187–92. http://dx.doi.org/10.1016/j.ifacol.2019.12.256.
[6] Allen E. Modeling with Itô stochastic differential equations. Math Model: Theory Appl 2007;22.
[7] Nipa Kaniz Fatema, Jang Sophia R-J, Allen Linda JS. The effect of demographic and environmental variability on disease outbreak for a dengue model with a seasonally varying vector population. Math Biosci 2021;331(108516). http://dx.doi.org/10.1016/j.mbs.2020.108516.
[8] Xiu D. Numerical methods for stochastic computations: A spectral method approach. Cambridge texts in applied mathematics, New York: Princeton University Press; 2010.
[9] Smith RC. Uncertainty quantification: Theory, implementation, and applications. SIAM; 2013.
[10] Hussein A, Selim MM. Solution of the stochastic generalized shallow-water wave equation using RVT technique. Eur Phys J Plus 2015;130(12):249.
[11] Slama H, El-Bedwhey NA, El-Depsy A, Selim MM. Solution of the finite milne problem in stochastic media with RVT technique. Eur Phys J Plus 2017;132(12):505.
[12] Hussein A, Selim MM. A general probabilistic solution of randomized radioactive decay chain (RDC) model using RVT technique. Eur Phys J Plus 2020;135(5):418.
[13] Dorini FA, Cecconello MS, Dorini LB. On the logistic equation subject to uncertainties in the environmental carrying capacity and initial population density. Commun Nonlinear Sci Numer Simul 2016;33:160–73.

[14] Dorini FA, Bobko N, Dorini LB. A note on the logistic equation subject to uncertainties in parameters. Comput Appl Math 2018;37(2):1496–506.

[15] Kozin F. On the probability densities of the output of some random systems. J Appl Mech 1961;28:161–5.

[16] Saaty T. Modern nonlinear equations. New York: Dover Publications; 1981.

[17] Ehrendorfer M. The Liouville equation and its potential usefulness for the prediction of forecast skill. Part II: Applications. Mon Weather Rev 1994;122(4):714–28.

[18] Chen JB, Li J. A note on the principle of preservation of probability and probability density evolution equation. Probab Eng Mech 2009;24(1):51–9.

[19] Halder A, Bhattacharya R. Dispersion analysis in hypersonic flight during planetary entry using stochastic Liouville equation. J Guid Control Dynam 2011;34(2):459–74.

[20] Bevia V, Burgos C, Cortés JC, Navarro-Quiles A, Villanueva RJ. Uncertainty quantification analysis of the biological gompertz model subject to random fluctuations in all its parameters. Chaos Solitons Fractals 2020;138:109908.

[21] Tarasov VE. Exact solutions of Bernoulli and logistic fractional differential equations with power law coefficients. Mathematics 2020;8:2231. http://dx.doi.org/10.3390/math8122231.

[22] Area I, Nieto JJ. Power series solution of the fractional logistic equation. Physica A 2021;573:125947. http://dx.doi.org/10.1016/j.physa.2021.125947.

[23] Consolini G, Materassi M. A stretched logistic equation for pandemic spreading. Chaos Solitons Fractals 2020;140:110113. http://dx.doi.org/10.1016/j.chaos.2020.110113.

[24] Winsor CP. The Gompertz curve as a growth curve. Proc Natl Acad Sci 1932;18(1):1–8. http://dx.doi.org/10.1073/pnas.18.1.1.

[25] Koya P, Goshu A. Generalized mathematical model for biological growths. Open J Model Simul 2013;1:42–53. http://dx.doi.org/10.4236/ojmsi.2013.14008.

[26] Marusic M, Bajzer Z, Vuk-Pavlovic S, Freyer JP. Tumor growth in vivo and as multicellular spheroids compared by mathematical models. Bull Math Biol 1994;56:617–31.

[27] Spratt JS, Meyer JS, Spratt JA. Rates of growth of human neoplasms: Part II. J Surg Oncol 1996;61(1):68–83.

[28] Birch CP. A new generalized logistic sigmoid growth equation compared with the Richards growth equation. Ann Botany 1999;83(6):713–23.

[29] Sachs RK, Hlatky LR, Hahnfeldt P. Simple ODE models of tumor growth and anti-angiogenic or radiation treatment. Math Comput Modelling 2001;33(12–13):1297–305.

[30] Hsieh YH, Lee JY, Chang HL. SARS epidemiology modeling. Emerg Infect Diseases 2004;10(6):1165.

[31] Hsieh YH. Richards model: a simple procedure for real-time prediction of outbreak severity. In: Modeling and dynamics of infectious diseases. World Scientific; 2009, p. 216–36.

[32] Hsieh YH, Ma S. Intervention measures, turning point, and reproduction number for dengue, Singapore, 2005. Am J Trop Med Hyg 2009;80(1):66–71.

[33] Hsieh YH. Pandemic influenza A (H1N1) during winter influenza season in the southern hemisphere. Influenza Other Respir Viruses 2010;4(4):187–97.

[34] Chowell G, Hincapie-Palacio D, Ospina JF, Pell B, Tariq A, Dahal S, Moghadas SM, Smirnova A, Simonsen L, Viboud C. Using phenomenological models to characterize transmissibility and forecast patterns and final burden of Zika epidemics. PLoS Curr 2016;8.

[35] Pell B, Kuang Y, Viboud C, Chowell G. Using phenomenological models for forecasting the 2015 Ebola challenge. Epidemics 2018;22:62–70.

[36] Pelinovsky E, Kurkin A, Kurkina O, Kokoulina M, Epifanova A. Logistic equation and COVID-19. Chaos Solitons Fractals 2020;140:110241.

[37] Wu K, Darcet D, Wang Q, Sornette D. Generalized logistic growth modeling of the COVID-19 outbreak: comparing the dynamics in the 29 provinces in China and in the rest of the world. Nonlinear Dynam 2020;101(3):1561–81.

[38] Aviv-Sharon E, Aharoni A. Generalized logistic growth modeling of the COVID-19 pandemic in Asia. Infect Dis Model 2020;5:502–9.

[39] Lee SY, Lei B, Mallick B. Estimation of COVID-19 spread curves integrating global data and borrowing information. PLoS One 2020;15(7):e0236860.

[40] McShane EJ. Extension of range of functions. Bull Amer Math Soc 1934;40(12):837–42.

[41] Strand JL. Random ordinary differential equations. J Differential Equations 1970;7(3):538–53.

[42] Casella G, Berger RL. Statistical inference. 2nd ed.. Duxbury, Pacific Grove; 2002.

[43] Calatayud J, Jornet M. Extending the applicability of the RVT technique for the randomized radioactive decay chain model. Eur Phys J Plus 2022;137:405. http://dx.doi.org/10.1140/epjp/s13360-022-02625-7.

[44] Rudin W. Principles of mathematical analysis. International series in pure & applied mathematics, 3rd ed.. 1976.

[45] Williams D. Probability with martingales. New York: Cambridge University Press; 1991.

[46] Scheffé H. A useful convergence theorem for probability distributions. Ann Math Stat 1947;18(3):434–8.

[47] Evans LC. Partial differential equations. Providence, R.I.: American Mathematical Society; 2010.

[48] Dimarco G, Loubère R, Narski J, Rey T. An efficient numerical method for solving the Boltzmann equation in multidimensions. J Comput Phys 2018;353:46–81. http://dx.doi.org/10.1016/j.jcp.2017.10.010, ff.ffhal-01357112.

[49] Butcher JC. Numerical methods for ordinary differential equations. New York: John Wiley and Sons; 2008.

[50] Bergdorf M, Koumoutsakos P. A Lagrangian particle-wavelet method. Multiscale Model Simul 2006;5(3):980–95. http://dx.doi.org/10.1137/060652877.

[51] Wang D, Tan D, Liu L. Particle swarm optimization algorithm: an overview. Soft Comput 2018;22:387–408. http://dx.doi.org/10.1007/s00500-016-2474-6.

[52] Burgos-Simón C, Cortés JC, Martínez-Rodríguez D, et al. Modeling breast tumor growth by a randomized logistic model: A computational approach to treat uncertainties via probability densities. Eur Phys J Plus 2020;135:826. http://dx.doi.org/10.1140/epjp/s13360-020-00853-3.

[53] Jaynes ET. Information theory and statistical mechanics. Phys Rev 1957;106:620–30. http://dx.doi.org/10.1103/PhysRev.106.620.

[54] Michalowicz JV, Nichols JM, Bucholtz F. Handbook of differential entropy. Chapman and Hall/CRC; 2013.

[55] Luenberger DG. Optimization by vector space methods. 1st ed.. USA: John Wiley and Sons, Inc.; 1997.

[56] Ram Y, Dellus-Gur E, Bibi M, Karkare K, Obolski U, Feldman MW, Cooper TF, Berman J, Hadany L. Predicting microbial growth in a mixed culture from growth curve data. Proc Natl Acad Sci USA 2019;116:14698–707. http://dx.doi.org/10.1073/pnas.1902217116.